MOTION GENERATION FOR A HUMANOID ROBOT WITH INLINE-SKATE

Nir Ziv*, Yong Kwun Lee* and Gaetano Ciaravella**
*Center for Cogntive Robotics, University of Science and Technology (UST) & Korea Institute of Science and Technology (KIST), 39-1 Hawolgol-Dong, Wolsong-Gil 5, Seongbuk-gu, Seoul, South Korea
**Cognative Center for Robotic Research, Korea Institute of Science and Technology (KIST), Seoul, South Korea

Keywords: Humanoid, Inline-Skate, Skating Motion, Wheeled Locomotion.

Abstract: A lot of research has been done for bipedal walking and many positive results have been produced, such as the ASIMO robot from Honda. However, although bipedal walking is a good solution for moving over uneven surfaces; bipedal walking is inefficient over an even surface because the robot's walking speed and stability are limited. Consequently, employing a wheeled locomotion on even surfaces can be advantageous. This paper presents a mathematical model and simulation of wheeled biped robot with two passive wheels on each foot. This enables the robot to move more efficiently over even surfaces. Also, this paper attempts to produce a more human-like inline-skating motion than previously created inline-skating simulations.

1 INTRODUCTION

Over the last few years, research on bipedal walking has progressed and has lead to major successes within the robotics field. One good example of this success is the ASIMO robot, a Honda creation. At the time of writing this paper, ASIMO can run with a speed of 6 km/h and is able to walk at a speed of 2.7 km/h (Honda). When considering the strongest achievements which leg locomotion has achieved until now, one major progressive accomplishment has been the ability for robots to move across uneven surfaces.

However, when considering robotic leg locomotion across only even tarains, the advantages of wheeled locomotion are greater than bipedal (or leg) locomotion. The reason for this is because the wheeled robot's moving speed and efficiancy are stronger and more stable. This is because leg locomotion algorithms are more complex than wheeled motion, making it more difficult for bipedal robots to walk or run quickly. (Jo et al 2008).

Therefore, to combine the advantages of both leg and wheeled locomotion, hybrid robot systems were developed. For example, WorkPartner is a quadruped system that can detect the type of surface it is on, even or uneven, and can then choose accordingly the type of locomotion to use, wheeled or bipedal (Ylonen et al 2002). Another example of hybrid locomotion is WS-2/ WL-16 (Waseda Shoes – Number 2 / Waseda Leg – Number 16) (Hashimoto et al 2005) which also combines bipedal walking with wheeled locomotion. Both WorkPartner and WS-2/WL-16 use DC motorized wheels.

However, because both WorkPartner and WS-2/WL-16 utilize motor wheels, this means that the brake and steering are also motorized. As a result, a robot with motorized wheels has larger wheels and its robotic system becomes heavier and, therefore, less agile.

To solve this issue, passive wheel locomotion has been suggested. One example of a hybrid, passive wheeled robot is the Roller-walker, developed by Hirose and Takeuchi (Hirose et al 1996, 1999, 2000.) In this system, the wheel motion is not generated by a DC motor, instead the robot moves by making a roller skating-like motion. Another example of passive wheel locomotion is the Rollerblader (Chitta et al 2003), which has two passive wheels that move in symmetric and anti-symmetric motions to propel the Rollerblader forward and in a rotary motion respectively.

Similarly, in this paper we present a simulation of a passive wheeled robot to generate a forward motion; our robot consists of two legs with two passive wheels attached along the middle of each

Ziv N., Lee Y. and Ciaravella G. (2010).
MOTION GENERATION FOR A HUMANOID ROBOT WITH INLINE-SKATE.
In *Proceedings of the 7th International Conference on Informatics in Control, Automation and Robotics*, pages 354-359

foot. However, unlike the Rollerblader, our simulation and model will attempt to create a more human-like motion using 'D' shape movement for the pushing leg where near the end of the movement the pushing leg will be raised in the air.

This paper is organized as follows. The following section will describe the modelling and the equations of the robot's motion. In section 3, we will show the simulation, motion steps and results. We will conclude with a brief discussion about the simulation's results, as well as problems that need to be solved within further research in the future.

2 MODELLING

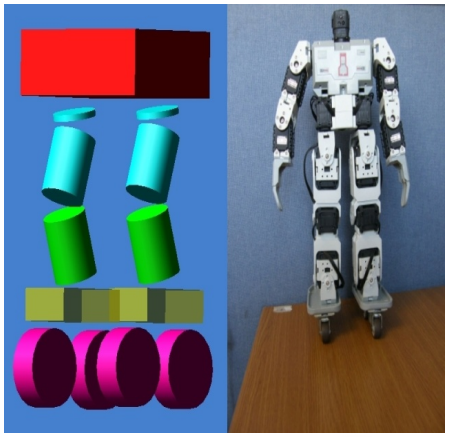

Figure 1: MSC.ADAMS Model and Read Small Size Humanoid.

The modelling of the robot (figure 1) was done by using MSC.ADAMS software. The robot has a total of 12 Degrees Of Freedom (DOF), where each leg contains 6 DOF. Two passive wheels were added to each foot along the middle of the foot.

The forces acting on the robot configuration (figure 2) and a derivation of the equations of motion are shown and explained in more detail in the next section.

2.1 Parametric Modelling

Solving the equations of motion for this system is a very complex process; therefore, the following few assumptions were made:

- Even though the motion is continuous, we will solve it for a time equal to t (where t is a segment of the whole motion.)
- External force, such as air resistance, external push and wind are negligible.
- The simulation motion is a forward motion. This will reduce the amount of forces acting on the model for rotational motion.

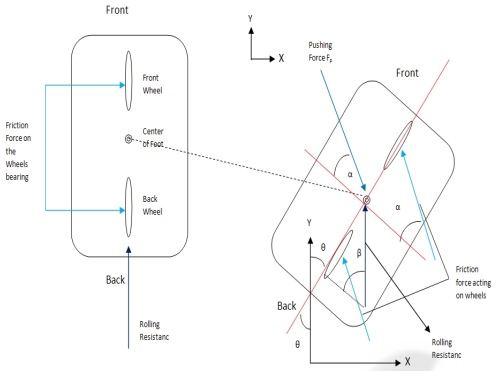

Figure 2: Forces Acting on the Robot.

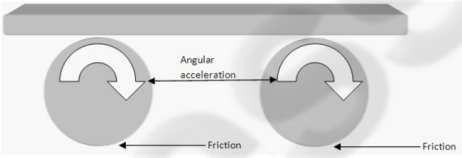

Figure 3: Side View of the Forces Acting on the Robot.

Because we are trying to simulate a forward motion, the forces acting on the model should satisfy the following equations:

$$\sum F_x = 0 \tag{1}$$

$$\sum \mathrm{F_y} = \mathrm{M_t} * \ddot{y} \tag{2}$$

Where F_x and F_y are the forces acting on the X axis and Y axis respectively. M_t is the total mass and $\ddot{y}$ is acceleration. As figure 2 shows, we will calculate the forces that act on the model.

First, we will analyze the stationary foot. Figure 2 shows the robot's stationary foot as the left foot.

$$\begin{aligned} F_r &= C_{rr} * N \\ \mathrm{N} &= \mathrm{M_t} * \mathrm{g} \end{aligned} \tag{3}$$

Where F_r, C_{rr} and N are the rolling resistance force, the rolling resistance coefficient and the normal force respectively (Peck et al 1859,National Research council 2006) and, in this instance, the normal force is total mass (M_t) times gravity (g).

$$\begin{aligned} F_{fs} &= \mu_f * N \\ N &= M_t * g \end{aligned} \tag{4}$$

Where F_{fs} is the frictional force on the stationary

foot, μ_f is the friction coefficient, N is the normal force, M_t is the total mass and g is the gravitational force.

Because the stationary foot will always point forward (there is no Z axis rotation) and the foot will be perpendicular to the ground, the rolling resistance force will always act on the Y axis. The frictional force from equation (4) will be used for the wheels' momentum as described next.

The last force acting on the stationary foot is the wheels momentum force. This can be seen in figure 3. The force acting on the wheels can be expressed as follows:

$$MO_w = I * \ddot{\theta} - F_{fs} * r \tag{5}$$

MO_w is single wheel momentum, I is the inertial mass, $\ddot{\theta}$ is angular acceleration F_{fs} is frictional force on the stationary foot and r is the wheel radius. Because we have two wheels on each foot, we can express equation (5) as follows:

$$MO_t = 2 * \left(\frac{I*\ddot{\theta}}{r} - F_{fs}\right) \tag{6}$$

MO_t is the total momentum force acting on the stationary foot's wheels.

Until now we have described the forces which are acting on the stationary foot (or the left foot from figure 2). Now we will describe in the same manner the forces acting on the pushing foot (or the right foot from figure 2).

First, we will look at the pushing force. The pushing force will act on the pushing leg with an angle of α. This angle will vary with time. However, as stated earlier to simplify the equations, we assume that we are looking at a given time t and therefore remove the dependency of time.

Because the pushing force is acting with an angle, we will need to derive the X and Y component of this force. These components are as follows:

$$\begin{aligned} F_{px} &= F_p * \cos\alpha \\ F_{py} &= F_p * \sin\alpha \end{aligned} \tag{7}$$

F_{px} and F_{py} are the pushing forces on the X axis and the Y axis respectively. F_p is the pushing force and α is the angle between the pushing force and the pushing foot.

As a reaction force to the pushing force, the pushing foot will experience a frictional force as well. This force can be written as:

$$\begin{aligned} F_{fp} &= \mu_f * N \\ N &= M_t * g + F_p * \sin\alpha + F_r * \cos\beta \end{aligned} \tag{8}$$

As with the pushing force, we will need to work on the X axis and Y axis components of the friction force. Using equation 8 with angle α produces the following equations:

$$\begin{aligned} F_{fpx} &= F_{fp} * \cos\alpha \\ F_{fpy} &= F_{fp} * \sin\alpha \end{aligned} \tag{9}$$

Where F_{fpx} is the frictional force on the pushing foot on the X axis and F_{fpy} is on the Y axis.

Using equations (1) and (2) and summing all the forces that act on the X axis and Y axis, we can rewrite equations (1) and (2) as follows:

$$\begin{aligned} \sum F_x &= 0 \\ [F_p - F_{fp}] * \cos\alpha &= 0 \end{aligned} \tag{10}$$

$$\begin{aligned} \sum F_y &= M_t * \ddot{y} \\ MO_t + F_r + [F_p - F_{fp}] * \sin\alpha &= M_t * \ddot{y} \end{aligned} \tag{11}$$

Using equations (3) – (9) and solving equation (11) for $\ddot{y}$, we can rewrite equation (11) as follows:

$$MO_t + F_r + [F_p - F_{fp}] * \sin\alpha = M_t * \ddot{y} \tag{12}$$

$$\frac{MO_t}{M_t} + \frac{F_r}{M_t} + \frac{F_p * \sin\alpha}{M_t} - \frac{F_{fp}\sin\alpha}{M_t} = \ddot{y} \tag{13}$$

$$F_p\left[\frac{\sin\alpha - \mu_f * \sin\alpha * \sin\alpha}{M_t}\right] + \frac{2*I*\ddot{\theta}}{M_t * r} + \mu_f * g\left[-2 + \frac{C_{rr}}{\mu_f} - \sin\alpha - C_{rr} * \cos\theta * \sin\alpha\right] = \ddot{y} \tag{14}$$

$$F_p\left[\frac{\sin\alpha - \mu_f * \sin\alpha * \sin\alpha}{M_t}\right] + C_1 * \ddot{\theta} + C_3[-2 + C_2 - \sin\alpha - C_{rr} * \cos\theta * \sin\alpha] = \ddot{y} \tag{15}$$

$$\ddot{y} = \frac{F_p*(\sin\alpha - \mu_f * \sin\alpha * \sin\alpha)}{M_t} + C_1\ddot{\theta} - C_2[2 - C_3 + \sin\alpha + C_{rr} * \cos\beta * \sin\alpha] \tag{16}$$

Where $C_1 = \frac{2*I}{M_t * r}$, $C_2 = \mu_f * g$ and $C_3 = \frac{C_{rr}}{\mu_f}$. For a full derivation of how we developed equation (12), please refer to the appendix.

2.2 Model Analysis

From equation (16) above, we notice that in order to make the acceleration higher, and therefore make the robot move forward faster, we needed to identify a few components of the equation and check the values that qualify our needs.

Equation (16) can be written in simple form as follows:

$$\ddot{y} = A + B * \ddot{\theta} - C \tag{17}$$

Where:

$$A = \frac{F_p*(\sin\alpha - \mu_f*\sin\alpha*\sin\alpha)}{M_t} \quad (18)$$

$$B = \frac{2*I}{M_t*r} \quad (19)$$

$$C = -C_2[2 - C_3 + \sin\alpha + C_{rr} * \cos\beta * \sin\alpha] \quad (20)$$

In order to make ÿ bigger, we must make A and B bigger and make C as small as possible. To make equation (18) bigger, we identified α as the variable since F_p, M_t and μ are constants. Using this notion, we plotted equation (18) into Matlab. The results are shown in figure 4.

As can be seen in figure 4, which shows when α is static and not dynamically changed by time, the value of α that will be the best in order to make the pushing force greatest (i.e. part A) is $\alpha = \frac{\pi}{2}$ or ,in other words, when $\alpha = 90^o$. At the same time, the best value for μ is 0.2. When looking in detail at equation (20), we identified α and β as the variables because the rest of equation (20) is constant. Because we already determined the value of α from equation (18), we will need to find the best value of β. Using the same value of α with β, we will succeed to minimize equation (20) since cos (90^o) will make the last part of C equal to zero.

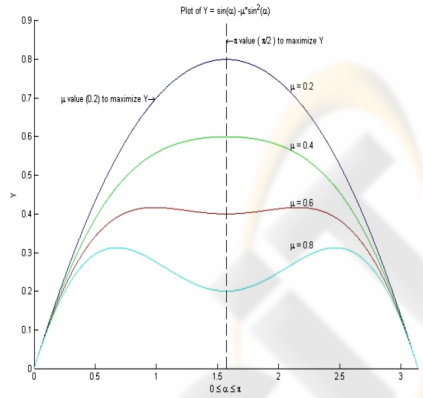

Figure 4: Matlab Plotting the relationship between values of μ and α to maximize pushing force.

The middle part of equation (18) is shown in equation (19) and has been plotted in Matlab; it can be seen in figure 5. In figure 5, we showed the relationship between the angular acceleration, $\ddot{\theta}$, and the robot acceleration, ÿ. As expected, the relationship between the two accelerations is linear, which means that the faster the angular acceleration on the wheels will be, the faster the robot acceleration will be. Also, we verified the equations with different values of the pushing force.

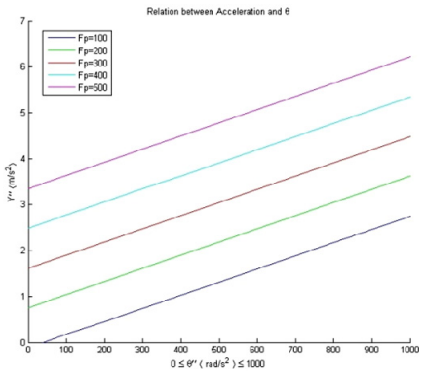

Figure 5: Matlab plotting the relationship between acceleration and angular acceleration.

3 SIMULATION

We used MSC.ADAMS to simulate the skating motion. The model is a simple model of the real humanoid (see figure 1) and the motions were generated by using three general motions that act on the model (one general motion on the hip with relation to the ground, one general motion on the left leg with relation to the hip and the last general motion on the right leg with relation to the hip as well). With these three general motions we controlled the angles or the joint and displacements of the rigid bodies. The skating motion is combined of six steps, three for the right foot, and three for the left foot to produce a full cycle of motion.

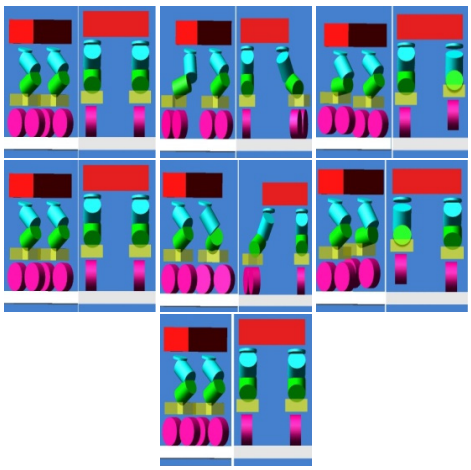

Figure 6: The Simulation Algorithm Sequence. The left image in each square shows the view from the side and the image on the right shows the view from the back.

The shape of the pushing leg motion is like a ‘D’

shape, starting from the top left corner and can be viewed in two parts. In the first part, the pushing leg is on the ground and is moving in slow motion. In the second part, the pushing leg is in the air and to maintain balance this step part is faster than the first part of the cycle.

The following are the motion steps (assuming that we begin with the right foot):

1. To start, the right foot is pushed away from the body, creating a 'D' shape
2. Before the 'D' is completed, the right foot is returned to the ground and a triangle shape between the pushing leg, body and stationary leg is formed.
3. Then the pushing leg is lifted and returned to its starting position, parallel to the stationary leg.
4. Step 1 is repeated, except that the left foot replaces the right foot.
5. Before the 'D' is completed, the left foot is returned to the ground and a triangle shape between the pushing leg (this time it is the left leg), body and stationary leg (this time it is the right leg) is formed.
6. Then the pushing leg is lifted and returned to its starting position, parallel to the stationary leg.

One can note that steps 4-6 are a mirror of steps 1-3. Figure 6 shows the images of these 6 steps. Notice the top right image from figure 6 where the triangle between the pushing leg, body and stationary foot is formed.

The time interval for the simulation is 5 seconds with 100 frames. During that simulation the skating motion (steps 1-6) ran twice, this means that each leg creates the pushing force twice. The result of this run was that the robot created enough pushing force to overcome the friction and succeeded to create a forward motion.

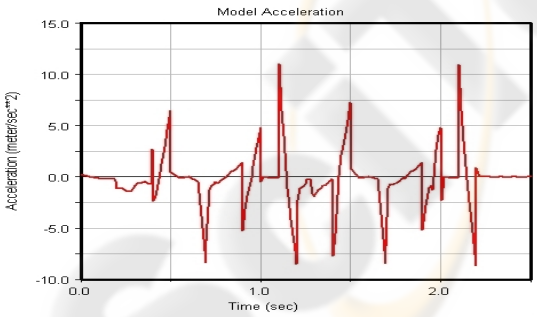

Figure 7: ADAMS Model Acceleration.

Figure 7 and figure 8 are showing the acceleration and angular acceleration of the model and a single wheel of the model respectively. These plots were taken from MSC.ADAMS software. Comparing these values to our Matlab plotting in figure 4 and figure 5 we can see that the results in both MSC.ADAMS simulation and our derivation of the equations of motion agree with one another. Both results show that as the acceleration increases the angular acceleration on the wheels will increase as well.

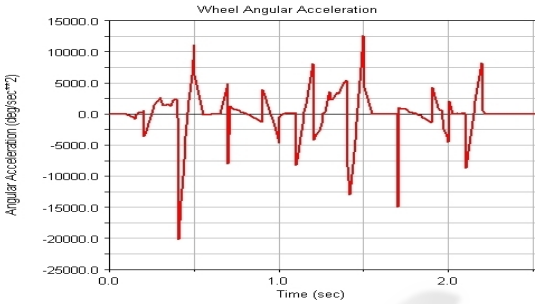

Figure 8: ADAMS Wheel Angular Acceleration.

4 CONCLUSIONS

This paper presents a simulation model with defined motion steps to generate a human-like skating motion. The simulation uses a robot which has two passive wheels on each foot along the middle of the foot. We successfully simulated the skating motion and generated a forward motion.

We also calculated the equations of motions for this model, and used Matlab to find a feasible value for dependent variables. The results were compared between the simulation and the mathematical model successfully. Even though this was a successful simulation, our next step will be to generate this motion in a real humanoid that follows the model, as can be seen in figure 9, figure 10 and figure 11. Additionally, researching a sounder algorithm to produce a more smooth 'D' shape would be valuable. Finally, further research would be to create a humanoid based on our model which would have the ability to transform itself between wheeled locomotion and leg locomotion depending on the surface it is crossing (even or uneven).

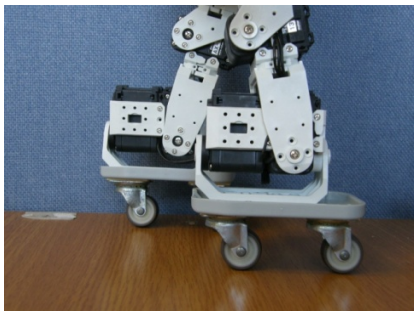

Figure 9: Small Size Humanoid Wheels.

Figure 10: Small Size Humanoid Front View.

Figure 11: Small Size Humanoid Side View.

REFERENCES

Chitta S., Kumar V., 2003. Dynamics and Generation of Gaits for a Planar Rollerblader. *International Conference of Intelligent Robots and Systems*.

Endo G., Hirose S., 1999. Study on Roller-Walker (System Integration and Basic Experiments.) *International Conference on Robotics and Automation*.

Endo G., Hirose S., 2000. Study on Roller-Walker (Multi-mode Steering control and Self-contained Locomotion.) *International Conference on Robotics and Automation.*

Hashimoto K., Hosobata K, Sugahara Y., Mikuriya Y, Lim H., Takanishi A., 2005. Realization by Biped Leg-wheeled Robot of Biped Walking and Wheel-driven Locomotion. *International Conference on Robotics and Automation.*

Hirose S., Takeuchi H., 1996. Study on roller-walker (Basic Characteristics and its Control.) *International conference on Robotics and Automotion.*

Honda, ASIMO, January, 13th 2010. *The New ASIMO – Major Features Summary*. http://www.hondauk-media.co.uk/uploads/presspacks/bf27134f6692b1c050d8ae9c29bc21840af2a723/Major_Features_Summary.pdf

Jo S., Chu J., Lee Y., 2008. Motion Planning for Biped Robot with Quad Roller Skates. *International conference on Control, Automation and System*.

National Research Council Special Report 286, 2006. Tires and Passengers Vehicle Fuel Economy. Washington D.C.

Peck William Guy , 1859. Element of Mechanics: For the Use of Colleges, Academics and High Schools. A.S. *Barnes & Burr. New York*

Ylonen S. J., Halme A. J., 2002. WorkPartner – Centaur like Service Robot. *Intl. Conference on Intelligent Robots and Systems*.